Inorganic Chemistry

Article

pubs.acs.org/IC

From $M(BH_4)_3$ (M = La, Ce) Borohydride Frameworks to Controllable Synthesis of Porous Hydrides and Ion Conductors

Morten Brix Ley,*[,†,‡] Mathias Jørgensen,[†] Radovan Černý,[§] Yaroslav Filinchuk,[∥] and Torben R. Jensen*[,†]

[†]Center for Materials Crystallography (CMC), Interdisciplinary Nanoscience Center (iNANO) and Department of Chemistry, University of Aarhus, Langelandsgade 140, DK-8000 Århus C, Denmark

[‡]Max-Planck-Institut für Kohlenforschung, Kaiser-Wilhelm-Platz 1, 45470 Mülheim an der Ruhr, Germany

[§]Laboratory of Crystallography, DQMP, University of Geneva, Quai Ernest-Ansermet 24, CH-1211 Geneva, Switzerland

[∥]Institute of Condensed Matter and Nanosciences, Université catholique de Louvain, Place L. Pasteur 1, 1348 Louvain-la-Neuve, Belgium

Supporting Information

ABSTRACT: Rare earth metal borohydrides show a number of interesting properties, e.g., Li ion conductivity and luminescence, and the series of materials is well explored. However, previous attempts to obtain $M(BH_4)_3$ (M = La, Ce) by reacting MCl_3 and $LiBH_4$ yielded $LiM(BH_4)_3Cl$. Here, a synthetic approach is presented, which allows the isolation of $M(BH_4)_3$ (M = La, Ce) via formation of intermediate complexes with dimethyl sulfide. The cubic c-$Ce(BH_4)_3$ ($Fm\bar{3}c$) is isostructural to high-temperature polymorphs of $A(BH_4)_3$ (A = Y, Sm, Er, Yb) borohydrides. The larger size of the Ce^{3+} ion makes the empty void in the open ReO_3-type framework structure potentially accessible to small guest molecules like H_2. Another new rhombohedral polymorph, r-$M(BH_4)_3$ (M = La, Ce), is a closed form of the framework, prone to stacking faults. The new compounds $M(BH_4)_3$ (M = La, Ce) can be combined with LiCl in an addition reaction to form $LiM(BH_4)_3Cl$ also known as $Li_4[M_4(BH_4)_{12}Cl_4]$; the latter contains the unique tetranuclear cluster $[M_4(BH_4)_{12}Cl_4]^{4-}$ and shows high Li-ion conductivity. This reaction pathway opens a way to synthesize a series of $A_4[M_4(BH_4)_{12}X_4]$ (M = La, Ce) compounds with different anions (X) and metal ions (A) and potentially high ion conductivity.

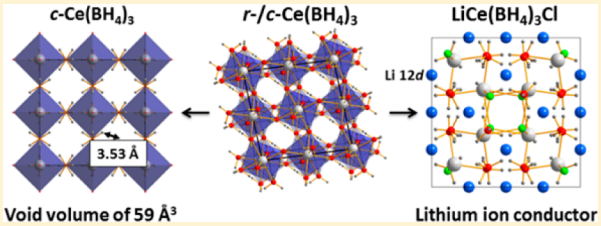

1. INTRODUCTION

A sustainable future requires a plentiful and inexpensive energy carrier.[1,2] Currently, lithium ion battery and hydrogen technologies are the two most promising options for mobile applications.[3−6] State-of-the-art fuel-cell vehicles presently employ high-pressure tanks (700 bar) for storing up to 5 wt % H_2.[2] The switch to solid-state hydrogen storage in complex hydrides would allow higher gravimetric and volumetric storage amounts.[7] Indeed, the potential of finding materials with extreme hydrogen densities was the initial spark that propelled researchers two decades ago to study complex hydrides.[8−10] Tank systems for solid-state hydrogen storage materials have received considerable attention, e.g., based on thermolysis of titanium catalyzed $NaAlH_4$ or hydrolysis of $NaBH_4$.[6,11] Unfortunately, hydrogen charging/discharging rates, high weight/large volume, and high costs still remain as challenges to be solved.[6] Continued research efforts on complex hydrides may help to overcome these barriers.

On the other hand, new applications of boron-based complex hydrides besides solid-state hydrogen storage have also attracted attention since the discovery of fast ionic conduction in lithium borohydride, $LiBH_4$.[12,13] Solid-state ion conductors may improve the safety and energy density of conventional lithium ion batteries.[14] The high-temperature hexagonal polymorph of $LiBH_4$ can be stabilized at room temperature by anion substitution with metal halides, and the composite system can be utilized in a battery at room temperature.[15,16] Ionic conductivity has also been discovered in materials containing higher boranes, e.g., $[B_{10}H_{10}]^{2-}$ or $[B_{12}H_{12}]^{2-}$,[17,18] and through combination of BH_4^- and $[B_{12}H_{12}]^{2-}$ containing compounds, suitable conductivities are now realized even close to room temperature.[19−21]

Lithium ion conductivity ($\sigma \approx 1 \times 10^{-4}$ S cm^{-1}) at room temperature has also been reported for mixed metal rare earth metal borohydrides, $LiM(BH_4)_3Cl$ (M = La, Ce).[22−24] $LiM(BH_4)_3Cl$ or $Li_4[M_4(BH_4)_{12}Cl_4]$ (M = La, Ce) contain the isolated tetranuclear anionic cluster $[M_4(BH_4)_{12}Cl_4]^{4-}$ with a distorted cubane M_4Cl_4 (M = La, Ce) core, which is charge balanced by Li^+ ions.[22,25] The $LiM(BH_4)_3Cl$ (M = La, Ce) structure has similarities with the known spinel structure.[26] With the recent discovery of perovskite metal borohydrides, photo physical and electronic properties were presented for rare earth metal borohydrides;[27] e.g., luminescence occurs both in $CsEu(BH_4)_3$ and $Eu(BH_4)_2(THF)_2$ (THF = tetrahydrofur-

Received: June 30, 2016
Published: September 13, 2016

DOI: 10.1021/acs.inorgchem.6b01526
Inorg. Chem. 2016, 55, 9748−9756

an).[27−29] Recently, also magnetocaloric effects have been measured in the bimetallic K−Gd metal borohydrides system.[30]

The availability of metal borohydrides with properties beyond hydrogen storage is in part owing to new synthesis methods that allow the removal of unwanted metal halide salts and production of unstable materials.[31−34] The rare earth metal borohydrides are usually synthesized by mechanochemistry, and many of the metal borohydrides containing metals from the sixth period of the periodic table and also scandium and yttrium were initially synthesized by this method.[35−37] In $M(BH_4)_3$, M = Y, Sm, Gd, Tb, Dy, Er, and Yb, the M^{3+} and BH_4^- ions are arranged in a distorted ReO_3-type structure at room temperature, while a face-centered cubic polymorph ($Fm\bar{3}c$) may crystallize at higher temperatures.[36−40] The metal ions, M = La, Ce, Pr, Nd, and Sm, with a radius larger than 0.983 Å have up to now only been described in the $LiM(BH_4)_3Cl$ structure.[22,23,26,37]

In this work, we investigate the synthesis of $M(BH_4)_3$ (M = La, Ce) using different solvents and determine the crystal structures of *r*-$M(BH_4)_3$ (M = La, Ce) (space group: $R\bar{3}c$, *r*: rhombohedral) and *c*-$Ce(BH_4)_3$ (space group $Fm\bar{3}c$, *c*: cubic). Finally, we present an addition reaction between *r*-$M(BH_4)_3$ (M = La, Ce) and LiCl leading to $LiM(BH_4)_3Cl$ (M = La, Ce), which provides a controllable synthesis pathway for other solid-state ion conductors.

2. EXPERIMENTAL SECTION

2.1. Synthesis. All preparations and manipulation of the samples were performed in a glovebox with a circulation purifier maintained under an argon atmosphere with <1 ppm of O_2 and H_2O or in dried glassware by Schlenk techniques. Lithium borohydride, $LiBH_4$ (Sigma-Aldrich 95%), lanthanum chloride, $LaCl_3$ (Sigma-Aldrich 99.9%), cerium chloride, $CeCl_3$ (Sigma-Aldrich 99.9%), toluene, $C_6H_5CH_3$ (Sigma-Aldrich, 99.8%), diethyl ether, Et_2O (Sigma-Aldrich, anhydrous, >99.0%) and dimethyl sulfide, $S(CH_3)_2$ (Sigma-Aldrich, anhydrous, >99.0%) were all used as received. All solid reactants were separately activated by ball milling in a Pulverisette 4 planetary ball mill for 12 repetitions applying 5 min milling and 2 min pause at a speed of 400 rpm using tungsten carbide balls and vials.

The synthesis of $LiM(BH_4)_3Cl$ (M = La, Ce) in Et_2O was performed by mixing MCl_3 (M = La, Ce) (n = 2 mmol) and $LiBH_4$ (n = 5 mmol) in 40 mL of Et_2O for 72 h at room temperature. A slight excess of the rare earth metal chloride is used to avoid $LiBH_4$ in the product. Following filtration, two immiscible phases were found, one of which was viscous. The viscous phase was difficult to filtrate properly and needed a longer time to flow through the filter. However, separation and drying of both phases revealed that $LiM(BH_4)_3Cl{\cdot}nEt_2O$ was present in both liquid phases.[41] Hereafter, the two phases were no longer separated. The excess solvent was removed by applying vacuum, and the solid $LiM(BH_4)_3Cl{\cdot}nEt_2O$ (M = La, Ce) phase was heated to 110 °C in dynamic vacuum ($p = 1 \times 10^{-3}$ bar) to produce $LiM(BH_4)_3Cl$ (M = La, Ce). The release of Et_2O from $LiM(BH_4)_3Cl{\cdot}nEt_2O$ (M = La, Ce) may be very quick, and solid material may easily escape the Schlenk equipment.

$M(BH_4)_3$ (M = La, Ce) is produced from MCl_3 (M = La, Ce) (n = 2 mmol) and $LiBH_4$ (n = 5 mmol) mixed in 40 mL of toluene for 72 h at room temperature. Again, a slight excess of the rare earth metal chloride is used to avoid unreacted $LiBH_4$. Afterward, the toluene solution is filtered off or removed *in vacuo*. $S(CH_3)_2$ (30 mL) is added to the solid mixture, whereby $M(BH_4)_3$ (M = La, Ce) is dissolved, while LiCl remains as a solid phase. After 24 h, the solution is filtered off and concentrated *in vacuo* leaving a solid $M(BH_4)_3{\cdot}nS(CH_3)_2$ (M = La, Ce) complex. $M(BH_4)_3{\cdot}nS(CH_3)_2$ (M = La, Ce) is heated to 120 °C in dynamic vacuum ($p = 1 \times 10^{-3}$ bar) leaving solid $M(BH_4)_3$ (M = La, Ce). Depending on how well the reactants are activated by ball milling, the reaction in toluene may benefit from heating under reflux at 90 °C for 5 h after the reaction at room temperature, followed by the same separation process in $S(CH_3)_2$. A sample of *r*-$La(BH_4)_3$-LiCl 1:1 was produced by ball milling according to the procedure described above for the activation of the reactants.

2.2. In Situ Time-Resolved Synchrotron Radiation Powder X-ray Diffraction. All air-sensitive samples were packed in a glovebox in either 0.5 mm glass capillaries sealed with glue or sapphire tubes (o.d. 1.1 mm, i.d. 0.8 mm).[42,43] *In situ* time-resolved synchrotron radiation powder X-ray diffraction data (SR-PXD) were collected at multiple synchrotrons. Data sets for $LiCe(BH_4)_3Cl{\cdot}nEt_2O$ and $Ce(BH_4)_3{\cdot}nS(CH_3)_2$ were collected at the Swiss-Norwegian Beamlines (BM01A, SNBL) at the European Synchrotron Radiation Facility (ESRF) in Grenoble, France, with a Pilatus area detector and λ = 0.688423 Å. The capillaries were oscillated by 30° during 30 s exposure of the samples to the X-ray beam. Data sets for $La(BH_4)_3{\cdot}nS(CH_3)_2$ and $La(BH_4)_3$ were collected at beamline I11 at the Diamond Light Source, Didcot, U.K. with a MythenII detector and λ = 0.827120 Å. The capillary was continuously oscillated during 30 s exposure of the sample to the X-ray beam. A data set was collected for $LiCe(BH_4)_3Cl{\cdot}nEt_2O$ at beamline I711 at the MAX-II synchrotron, MAX IV laboratory, Lund, Sweden, with a MAR165 CCD detector and λ = 0.9919 Å (sample packed in a sapphire tube). A data set for *r*-$La(BH_4)_3$ and *r*-$La(BH_4)_3$-LiCl 1:1 was collected at beamline P02.1 at PETRA III, DESY, Hamburg, Germany, with a PerkinElmer XRD 1621 detector system and λ = 0.2309 Å (sample packed in a sapphire tube). The glass capillaries or sapphire tubes containing the samples were usually heated from room temperature to 300 °C at $\Delta T/\Delta t$ = 5 °C/min, while SR-PXD data were collected.[33]

All obtained raw images were transformed to two-dimensional (2D) powder patterns using the FIT2D program,[34] and calibration measurements of the standard NIST LaB_6 sample, masking diffraction spots from the single-crystal sapphire sample holder. Uncertainties of the integrated intensities were calculated at each 2θ-point by applying Poisson statistics to the intensity data, considering the geometry of the detector.[35]

2.3. Structural Solution and Refinement of *r*-$Ce(BH_4)_3$, *c*-$Ce(BH_4)_3$, and *r*-$La(BH_4)_3$. The crystal structures of *r*-$Ce(BH_4)_3$ and *c*-$Ce(BH_4)_3$ were solved and refined from the same SR-PXD data set collected at 180 °C at BM01A, SNBL, ESRF. The unit cell of *r*-$Ce(BH_4)_3$ was indexed in DICVOL[44] and subsequently solved by global optimization in direct space in the program FOX.[45] The structural models of both compounds were refined by the Rietveld method using the program Fullprof.[46] The scattering powers differ significantly between the heavy atoms cerium and lanthanum compared to boron and hydrogen. Therefore, constraints were applied to the distances (B−H, 1.22 Å) and angles (H1−B−H2, 109.44°) between boron and hydrogen during the refinement for *r*-$Ce(BH_4)_3$. Despite the constraints, a small deformation is observed of the BH_4^- tetrahedron after the refinement. The final refinement parameters are R_p = 0.888%, R_{wp} = 1.75% (not corrected for background), R_p = 8.81%, R_{wp} = 8.64% (conventional Rietveld R-factors), R_{Bragg}(*r*-$Ce(BH_4)_3$) = 1.56%, R_{Bragg}(*c*-$Ce(BH_4)_3$) = 5.62%, and global χ^2 = 83.2; see Figure 1. The crystal structure of *c*-$Ce(BH_4)_3$ was checked with the program PLATON for empty voids.[47]

The crystal structure of *r*-$La(BH_4)_3$ was refined from a SR-PXD data set collected at room temperature after annealing at 140 °C at P02.1 at PETRA III, DESY, see Figure S1 (Supporting Information). The final refinement parameters for *r*-$La(BH_4)_3$ are R_p = 0.509%, R_{wp} = 1.08% (not corrected for background), R_p = 19.4%, R_{wp} = 17.7% (conventional Rietveld R-factors), R_{Bragg}(*r*-$La(BH_4)_3$) = 5.53% and global χ^2 = 282.

2.4. Thermal Analysis. Thermogravimetric analysis (TGA) and differential scanning calorimetry (DSC) were performed using either a PerkinElmer STA 6000 system or a Mettler Toledo TGA/DSC 1 STAR^e system. Mass spectrometry (MS) data were collected with a Hiden Analytical HPR-20 QMS sampling system. Each sample (approximately 5 mg) were placed in an Al crucible and heated from 40 to 450 °C (5 °C/min) with argon purge rate of 40 mL/min. The outlet gas species were monitored for hydrogen (m/z = 2), diborane (m/z = 26), dimethyl sulfide (m/z = 62), and/or diethyl ether (m/z = 74) using mass spectrometry.

DOI: 10.1021/acs.inorgchem.6b01526
Inorg. Chem. 2016, 55, 9748−9756

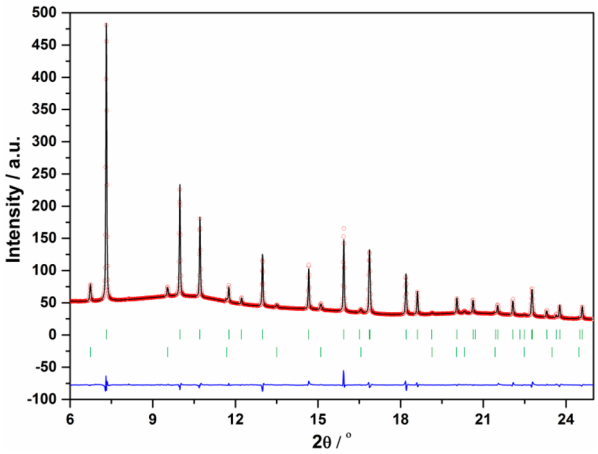

Figure 1. Rietveld refinement data for the mixture of *r*-$Ce(BH_4)_3$ and *c*-$Ce(BH_4)_3$ (beamline BM01A, SNBL, ESRF, λ = 0.688423 Å, T = 180 °C). Tick marks: top *r*-$Ce(BH_4)_3$ and bottom *c*-$Ce(BH_4)_3$.

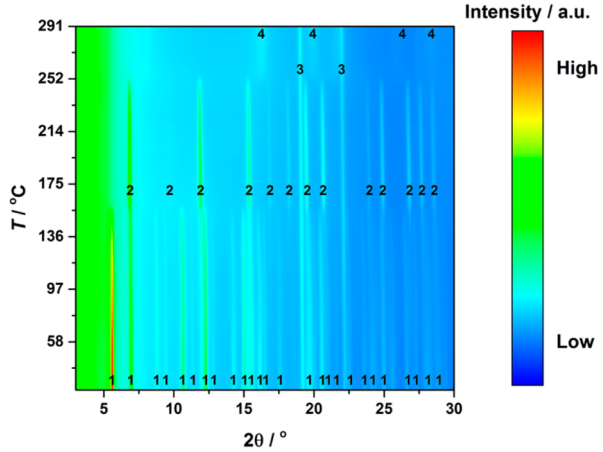

Figure 2. *In situ* SR-PXD data for $LiCe(BH_4)_3Cl{\cdot}nEt_2O$ (beamline I711, MAX II, MAXIV laboratory, λ = 0.9919 Å, $\Delta T/\Delta t$ = 5 °C/min, p(Ar) = 1 bar). Symbols: 1: $LiCe(BH_4)_3Cl{\cdot}nEt_2O$, 2: $LiCe(BH_4)_3Cl$, 3: LiCl, 4: Unknown.

3. RESULTS AND DISCUSSION

3.1. Synthesis of $LiM(BH_4)_3Cl$ (M = La, Ce) in Diethyl Ether. The reactions between MCl_3 (M = La, Ce) and $LiBH_4$ in either Et_2O or toluene/$S(CH_3)_2$ all produce metal borohydride phases. Therefore, in these reactions MCl_3 (M = La, Ce) are considered to behave alike owing to the comparable ionic size of La^{3+} and Ce^{3+}, 1.17 and 1.15 Å, respectively. The size of the rare earth metal ions usually determines the structure type of the obtained product in reactions between their respective chlorides and alkali metal borohydrides.[31,37] Mechanochemical treatment of MCl_3 (M = La, Ce) and $LiBH_4$ in both cases gives rise to $LiM(BH_4)_3Cl$, (M = La, Ce).[22,23] The reaction between MCl_3 (M = La, Ce) and $LiBH_4$ in Et_2O first produces an ether solvate, $LiM(BH_4)_3Cl{\cdot}nEt_2O$ (M = La, Ce), which upon removal of the coordinated solvent yields $LiM(BH_4)_3Cl$ (M = La, Ce) according to reaction 1 (shown for M = Ce).

$$CeCl_3(s) + 3LiBH_4(s) \xrightarrow[\mathbf{1.}\text{-}2LiCl]{\mathbf{1.}Et_2O,\text{filt.}} LiCe(BH_4)_3Cl{\cdot}nEt_2O(sol) \xrightarrow[\mathbf{2.}-Et_2O]{\mathbf{2.}T=110\,^\circ C,\text{vac}} LiCe(BH_4)_3Cl(s) \quad (1)$$

3.2. Thermally Induced Changes for $LiM(BH_4)_3Cl{\cdot}nEt_2O$ (M = La, Ce). *In situ* SR-PXD data were collected for the $LiCe(BH_4)_3Cl{\cdot}nEt_2O$ sample after drying at room temperature; see Figure 2. Several unknown Bragg reflections are ascribed to the unknown structure of $LiCe(BH_4)_3Cl{\cdot}nEt_2O$. These reflections disappear at approximately 140 °C. Hereafter, reflections corresponding to $LiCe(BH_4)_3Cl$ appear, which remain until 210 °C. Bragg reflections from LiCl are present from room temperature to 250 °C, indicating that LiCl remains in the sample even after filtration. Once the Bragg reflections from $LiCe(BH_4)_3Cl$ vanish, a set of four broad Bragg reflections from an unidentified compound appear. Comparison with a previous study suggests that the peaks may belong to either CeH_2 or CeB_6.[22]

The Bragg reflections from $LiCe(BH_4)_3Cl{\cdot}nEt_2O$ were indexed in a tetragonal unit cell with space group symmetry $P4_2/nnm$ and unit cell parameters a = 11.4995 and c = 21.1294 Å. The Le Bail fit is shown in Figure S2 (Supporting Information). Ab initio structure solution was attempted with the program FOX using the cubane anion $[Ce_4(BH_4)_{12}Cl_4]^{4-}$, Li^+ and one Et_2O molecule as objects. However, while it seemed clear that the complex anion $[Ce_4(BH_4)_{12}Cl_4]^{4-}$ was indeed present, it was not possible to determine the coordination of the diethyl ether molecule.

Thermal analysis and mass spectrometry show the thermal events and gas release from $LiCe(BH_4)_3Cl{\cdot}nEt_2O$ in Figure S3 (Supporting Information). Between 80 and 110 °C, a mass loss of 19.5 wt% is observed together with a release of Et_2O and a small amount of B_2H_6, as observed by TGA and MS, respectively. A small endothermic event is observed at 103 °C. This may either correspond to a release of Et_2O from the sample or from a polymorphic phase change of leftover $LiBH_4$ in the sample. Between 205 and 285 °C, a two-step mass loss of 4 wt% follows that originates from the release of hydrogen. This is accompanied by two small endothermic events at 209 and 240 °C. The event at 209 °C may correspond to a reaction between the remaining $LiBH_4$ and $LiCe(BH_4)_3Cl$. The event at 240 °C corresponds to the decomposition of $LiCe(BH_4)_3Cl$.

The theoretical mass loss of one Et_2O molecule from $LiCe(BH_4)_3Cl{\cdot}Et_2O$ is 24.6 wt%. *In situ* SR-PXD data indicate that some LiCl remain in the sample, which may decrease the mass loss observed by thermal analysis, which was only 19.5 wt %. Therefore, the solvent phase of $LiCe(BH_4)_3Cl$ most likely contains one Et_2O molecule per formula unit, i.e., $LiCe(BH_4)_3Cl{\cdot}Et_2O$. However, as it was not possible to solve the structure of $LiCe(BH_4)_3Cl{\cdot}nEt_2O$, the exact amount of Et_2O contained within the compound remains unknown. $LiBH_4$ dissolves in Et_2O and if it is not consumed in the reaction with MCl_3 (M = La, Ce), it may remain in the solution during filtration. Usually, the reaction is performed with a slight excess of MCl_3 (M = La, Ce) compared to $LiBH_4$. Since $LiBH_4$ is dissolved during the reaction, this may facilitate the incorporation of Li^+ and Cl^- into product, i.e., $LiM(BH_4)_3Cl$ (M = La, Ce). Therefore, $M(BH_4)_3$ (M = La, Ce) is not produced in the reaction in diethyl ether compared to the reaction in toluene. The thermal analysis indicates that in order to remove Et_2O from $LiCe(BH_4)_3Cl{\cdot}nEt_2O$, the sample should be heated to 110 °C. Indeed, the reaction between MCl_3 (M = La, Ce) and $LiBH_4$ in diethyl ether is a convenient way of preparing $LiM(BH_4)_3Cl$ (M = La, Ce) with a reduced amount of LiCl compared to the mechanochemical synthesis.[22,23]

DOI: 10.1021/acs.inorgchem.6b01526
Inorg. Chem. 2016, 55, 9748−9756

3.3. Synthesis of $M(BH_4)_3$ (M = La, Ce) in Toluene and Dimethyl Sulfide. The synthesis of $Y(BH_4)_3$ has previously been reported from YCl_3 and $LiBH_4$ in a 2 M solution of dimethyl sulfide borane in toluene followed by extraction with $S(CH_3)_2$.[31] Here, the reaction between MCl_3 (M = La, Ce) and $LiBH_4$ is conducted in toluene. Since neither MCl_3 (M = La, Ce) nor $LiBH_4$ are dissolved in toluene, the reaction is slower than the reaction in Et_2O. $S(CH_3)_2$ may be used as a solvent for both the reaction and the separation. However, the low solubility of both MCl_3 (M = La, Ce) and $LiBH_4$ in $S(CH_3)_2$ combined with the low boiling point of $S(CH_3)_2$ and its repulsive odor, have kept us from using this procedure. The synthesis of $M(BH_4)_3$ (M = La, Ce) occurs according to reaction 2 (shown for M = Ce).

$$\mathrm{CeCl_3(s) + 3LiBH_4(s)} \xrightarrow[\mathbf{2.}-3\mathrm{LiCl}]{\mathbf{1.}\mathrm{Toluene}\ \mathbf{2.}\mathrm{S(CH_3)_2,filt.}} \mathrm{Ce(BH_4)_3{\cdot}}n\mathrm{S(CH_3)_2(sol)} \xrightarrow[\mathbf{3.}-S(\mathrm{CH_3})_2]{\mathbf{3.}T=140\,^\circ\mathrm{C,vac}} \mathrm{Ce(BH_4)_3(s)} \quad (2)$$

3.4. Thermally Induced Changes for $M(BH_4)_3{\cdot}nS(CH_3)_2$ and $M(BH_4)_3$ (M = La, Ce). Following the synthesis of $M(BH_4)_3{\cdot}nS(CH_3)_2$ (M = La, Ce), the samples were studied by thermal analysis and *in situ* SR-PXD. The *in situ* SR-PXD data from $Ce(BH_4)_3{\cdot}nS(CH_3)_2$ after the sample was dried at room temperature are shown in Figure 3. The data contain several

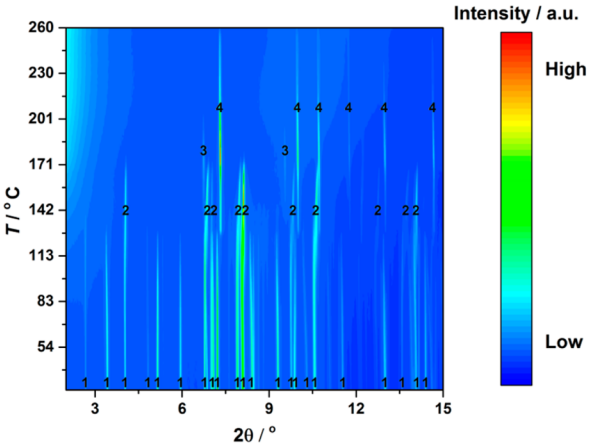

Figure 3. *In situ* SR-PXD data for $Ce(BH_4)_3{\cdot}nS(CH_3)_2$ (beamline BM01A, SNBL, ESRF, λ = 0.688423 Å, $\Delta T/\Delta t$ = 5 °C/min, p(Ar) = 1 bar). Symbols: 1: $Ce(BH_4)_3{\cdot}nS(CH_3)_2$, 2: $Ce(BH_4)_3{\cdot}mS(CH_3)_2$, 3: *c*-$Ce(BH_4)_3$, 4: *r*-$Ce(BH_4)_3$.

Bragg reflections denoted as group **1**. At the 129 °C, the reflections from **1** disappear and a new set of reflections denoted as group **2** become more obvious. **2** may be present already from room temperature. However, because of overlap between the reflections from **1** and **2**, the two phases are difficult to distinguish between room temperature and 140 °C. Bragg reflections from **2** disappear at 173 °C. At 129 °C, reflections corresponding to *r*-$Ce(BH_4)_3$ (**4**) already appear together with several small reflections from *c*-$Ce(BH_4)_3$ (**3**). Bragg reflections from *c*-$Ce(BH_4)_3$ (**3**) disappear at 200 °C, where it most likely is converted into *r*-$Ce(BH_4)_3$. Bragg reflections from *r*-$Ce(BH_4)_3$ (**4**) disappear at 260 °C.

Both **1** and **2** probably contain $S(CH_3)_2$ and their composition may be written as $Ce(BH_4)_3{\cdot}nS(CH_3)_2$ and $Ce(BH_4)_3{\cdot}mS(CH_3)_2$, where n and m correspond to different amounts of $S(CH_3)_2$. Indeed, Bragg reflections from *r*-$Ce(BH_4)_3$ (**4**) appear already when $Ce(BH_4)_3{\cdot}nS(CH_3)_2$ (**1**) disappear, and thus $S(CH_3)_2$ release from $Ce(BH_4)_3{\cdot}nS(CH_3)_2$ is expected to lead directly to *r*-$Ce(BH_4)_3$. Additionally, the intensity of the Bragg reflections from *r*-$Ce(BH_4)_3$ (**3**) increases further (173 °C) when the Bragg reflections from $Ce(BH_4)_3{\cdot}mS(CH_3)_2$ (**2**) disappear, indicating that $Ce(BH_4)_3{\cdot}mS(CH_3)_2$ may also release $S(CH_3)_2$ and form *r*-$Ce(BH_4)_3$. This supports that both $Ce(BH_4)_3{\cdot}nS(CH_3)_2$ and $Ce(BH_4)_3{\cdot}mS(CH_3)_2$ decompose into *r*-$Ce(BH_4)_3$. The formation of *c*-$Ce(BH_4)_3$ mostly occurs after the disappearance of $Ce(BH_4)_3{\cdot}mS(CH_3)_2$ (**2**). The claim that both **1** and **2** may contain $S(CH_3)_2$ is also supported by the mass loss and gas release for these samples recorded by thermal analysis and mass spectrometry discussed below.

In the different samples that have been prepared for $M(BH_4)_3{\cdot}nS(CH_3)_2$ (M = La, Ce) only Bragg reflections corresponding to **1** and **2** have been observed at room temperature by *in situ* SR-PXD. In some samples, **2** has been the major phase observed by X-ray diffraction, which during heating leads to *r*-$M(BH_4)_3$ (M = La, Ce). If the $M(BH_4)_3{\cdot}nS(CH_3)_2$ (M = La, Ce) samples are heated in a vacuum as described in the experimental section prior to the *in situ* SR-PXD experiment, only Bragg reflections from *r*-$M(BH_4)_3$ (M = La, Ce) are observed. Bragg reflections from *c*-$Ce(BH_4)_3$ have only been observed during *in situ* SR-PXD experiments, indicating the instability of this phase, as discussed below.

The structural description of $Ce(BH_4)_3{\cdot}nS(CH_3)_2$ (**1**) has not been possible, and attempts to index the Bragg reflections have not been successful. $M(BH_4)_3{\cdot}mS(CH_3)_2$ (M = La, Ce) (**2**) has been indexed in the hexagonal space group *P6/mmm* with unit cell parameters a = 11.2895(3) and c = 5.7926(2) Å. The Le Bail fit for $La(BH_4)_3{\cdot}mS(CH_3)_2$ is shown in Figure S4 (Supporting Information). *Ab initio* structure solution has been attempted in the program FOX with Ce^{3+}, BH_4^- and $S(CH_3)_2$ as starting objects. However, it was not possible to determine the crystal structure.

DSC and TGA data from $Ce(BH_4)_3{\cdot}nS(CH_3)_2$ are shown in Figure S5 (Supporting Information). A mass loss of 26 wt% is observed already from room temperature to 130 °C. This coincides with an endothermic process at 95 °C. These observations correspond well with the release of $S(CH_3)_2$ from $Ce(BH_4)_3{\cdot}nS(CH_3)_2$. The theoretical mass loss of one $S(CH_3)_2$ molecule from $Ce(BH_4)_3{\cdot}S(CH_3)_2$ is 25 wt%. Therefore, as for $Y(BH_4)_3{\cdot}S(CH_3)_2$, $M(BH_4)_3{\cdot}S(CH_3)_2$ (M = La, Ce) is the most probable composition.[31] Between 200 and 300 °C, another mass loss of 6 wt% is observed together with an endothermic process at 251 °C corresponding to the decomposition of *r*-$Ce(BH_4)_3$. The theoretical hydrogen content in *r*-$Ce(BH_4)_3$ is ρ_m = 6.5 wt% H_2. Thermal analysis data from *r*-$Ce(BH_4)_3$ after removal of $S(CH_3)_2$ is shown in Figure S6 (Supporting Information). Here, an endothermic process again occurs at 251 °C, while a mass loss of 8.5 wt% occurs between 200 and 300 °C. The mass loss may be slightly larger because of simultaneous release of B_2H_6.

The release of B_2H_6 is supported by thermal analysis and mass spectrometry experiments conducted for $La(BH_4)_3{\cdot}nS(CH_3)_2$; see Figure S7 (Supporting Information). Here, a release of B_2H_6 is recorded by MS between 250 and 275 °C. Additionally, three endothermic processes are observed at 60, 94, and 109 °C during release of $S(CH_3)_2$ from $La(BH_4)_3{\cdot}nS(CH_3)_2$. Indeed, this suggests that multiple different compositions containing $S(CH_3)_2$ exist for $M(BH_4)_3{\cdot}nS(CH_3)_2$

DOI: 10.1021/acs.inorgchem.6b01526
Inorg. Chem. 2016, 55, 9748−9756

(M = La, Ce) as discussed for the *in situ* SR-PXD data of $Ce(BH_4)_3 \cdot nS(CH_3)_2$; see Figure 3.

3.5. Crystal Structure of *r*-M(BH$_4$)$_3$ (M = La, Ce). *r*-$M(BH_4)_3$ (M = La, Ce) crystallizes in a trigonal crystal system with space group symmetry $R\bar{3}c$ and $Z = 6$. The final refinement was performed on SR-PXD data obtained at T = 180 °C at BM01A, SNBL, ESRF for *r*-$Ce(BH_4)_3$, see Figure 1, and for *r*-$La(BH_4)_3$ on SR-PXD data collected at room temperature after annealing at 140 °C at P02.1 at PETRA III, DESY; see Figure S1 (Supporting Information). The unit cell parameters of *r*-$Ce(BH_4)_3$ are a = 7.3745(1) Å and c = 20.1567(2) Å and for *r*-La(BH4)3 a = 7.2621(3) Å and c = 20.199(1) Å. In *r*-$Ce(BH_4)_3$, cerium is located on the 6b site, boron on the 18e site and hydrogen on two different 36f sites, see Table S1 (Supporting Information). The shortest Ce−H distances are Ce−H1 = 2.49(4) Å and Ce−H2 = 2.80(2) Å. The angle between Ce−B−Ce is 140.4(1)°. Six BH_4^- groups coordinate to each Ce ion through the faces of the BH_4^- tetrahedron; see Figure 4. The unit cell volumes, V/Z values and densities are shown in Table 1.

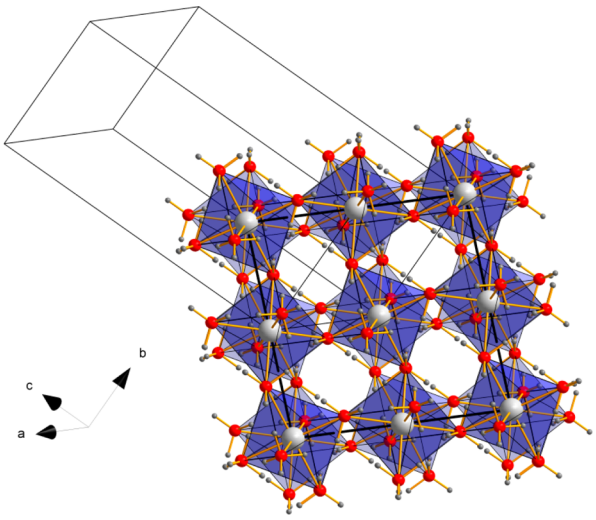

Figure 4. Structural representation the local environment around Ce in *r*-$Ce(BH_4)_3$ representing the tilts of $Ce(BH_4)_6$ octahedra and the relation between the cubic (shown by bold lines) and the hexagonal (thin lines) cells.

Some Bragg reflections are not explained by the unit cell of *r*-$Ce(BH_4)_3$; see Figure 1. A comparison of the Bragg reflections with the powder diffraction pattern of the high temperature β-$Y(BH_4)_3$ (space group $Fm\bar{3}c$) indicates that the Bragg reflections may belong to an unknown compound with a similar crystal structure to β-$Y(BH_4)_3$.[40] Because of the size difference between Y^{3+} (1.04 Å) and Ce^{3+} (1.15 Å), the Bragg reflections appear at correspondingly lower 2θ values. Indeed, Rietveld refinement confirms that the Bragg reflections belong to another polymorph of cerium borohydride, *c*-$Ce(BH_4)_3$, which crystallizes in a cubic unit cell with a = 11.7105(7) Å, Z = 8 and space group $Fm\bar{3}c$; see Table S2 (Supporting Information) and Figures 1 and 4. The unit cell volume and the crystallographic density of *c*-$Ce(BH_4)_3$ are shown in Table 1. A cubic polymorph for lanthanum borohydride has not been observed during the *in situ* SR-PXD studies of *r*-$La(BH_4)_3$.

The $R\bar{3}c$ structure of *r*-$Ce(BH_4)_3$ is a rhombohedral deformation of the $Fm\bar{3}c$ structure of *c*-$Ce(BH_4)_3$. The structural prototype of *r*-$M(BH_4)_3$ (M = La, Ce) is hp3-ReO_3.[38,39] The relation between hexagonal (H) and cubic (C) lattice parameters in the nondeformed cubic crystal is aH = (aC * sqrt(2))/2 and cH = aC * sqrt(3). Calculation of the nondeformed hexagonal unit cell parameters from the cubic unit cell parameters are aH = (11.71 Å * sqrt(2))/2 = 8.28 Å and cH = 11.71 Å * sqrt(3) = 20.28 Å. The values determined from Rietveld refinement of *r*-$Ce(BH_4)_3$ are aH = 7.3745(1) Å and cH = 20.1567(2) Å. The calculated values of aH and cH from aC show that the rhombohedral structure is strongly compressed along aH and expanded along cH. Hence, cerium is too big to keep the cubic $Fm\bar{3}c$ structure and the cubic frameworks collapses; the Ce−BH_4−Ce bridges are not straight anymore.

Several diffraction patterns collected on $M(BH_4)_3$ (M = La, Ce) in the early stages of the project could not be used for the structural solution because of the severe anisotropic line broadening; see Figure 5. In the end, diffraction patterns

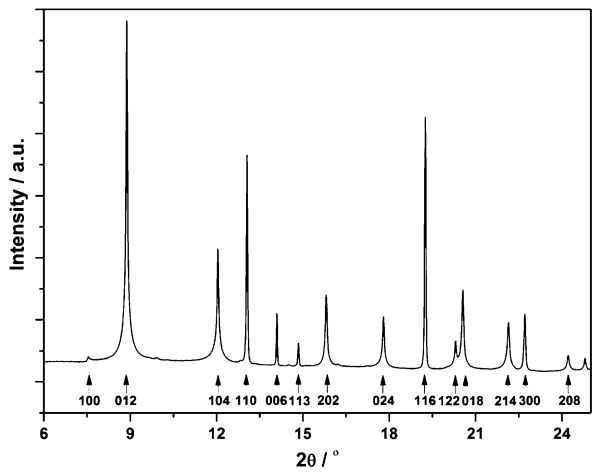

Figure 5. SR-PXD data for $La(BH_4)_3$ showing the anisotropic line broadening for specific reflections (beamline I11, Diamond, UK, λ = 0.827120 Å).

Table 1. Space Group, Ionic Radii, Unit Cell Volumes, Z, V/Z, and Densities for *r*-$La(BH_4)_3$, *r*-$Ce(BH_4)_3$, *c*-$Ce(BH_4)_3$, α-$Sm(BH_4)_3$, and β-$Sm(BH_4)_3$

	r-$La(BH_4)_3$	*r*-$Ce(BH_4)_3$	*c*-$Ce(BH_4)_3$	α-$Sm(BH_4)_3$[37]	β-$Sm(BH_4)_3$[37]
space group	$R\bar{3}c$	$R\bar{3}c$	$Fm\bar{3}c$	$Pa\bar{3}$	$Pm\bar{3}m$
ionic radii M^{3+}/Å	1.17	1.15	1.15	1.09	1.09
volume/Å^3	922.51(7)	949.33(1)	1605.9(2)	1366.1(9)	179.5(1)
Z	6	6	8	8	1
V/Z/Å^3	154	158	201	171	179
ρ/g/cm^3	1.981	1.938	1.527	1.895	1.803

DOI: 10.1021/acs.inorgchem.6b01526
Inorg. Chem. 2016, 55, 9748−9756

Table 2. Space Group, Unit Cell Parameter, Z, V/Z, Void Coordinates and Distance to Nearest H Atom for Different Framework Metal Borohydrides

compound	space group	unit cell parameter A/Å	Z	V/Z/Å^3	void coordinates	dist: void center to nearest H atom/Å	ref
c-$Ce(BH_4)_3$	$Fm\bar{3}c$	11.7105(7)	8	201	1/4, 1/4, 1/4	3.53	this work
β-$Y(BH_4)_3$	$Fm\bar{3}c$	11.0086(1)	8	167	1/4, 1/4, 1/4	3.32	36, 40
γ-$Mg(BH_4)_2$	$Id\bar{3}a$	15.7575(16)	24	163	1/8, 1/8, 1/8	3.56	49
γ-$Mn(BH_4)_2$	$Id\bar{3}a$	16.2094(13)	24	177	1/8, 1/8, 1/8	3.66	41

without anisotropic line broadening were collected for both $La(BH_4)_3$ and $Ce(BH_4)_3$ owing to annealing during the *in situ* SR-PXD experiments, which made the structural solution possible as discussed above. The strong anisotropic line broadening is caused by stacking faults on (001) planes in the hexagonal lattice, i.e., (111) planes in a cubic equivalent. It is a common case of faulting between *ccp* and *hcp*. By introducing hexagonal stacking faults on the planes (111) in the $Fm\bar{3}c$ model of c-$Ce(BH_4)_3$ and by transforming the cubic unit cell into a triple hexagonal cell, which is the $R\bar{3}c$ cell of r-$Ce(BH_4)_3$, the law which controls the broadening is according to Warren: H − K = 3n (no broadening) and H − K = 3n + 1 (broadening) (Miller indices in triple hexagonal cell).[48] That is what is observed in data obtained for $La(BH_4)_3$; see Figure 5. The broadening due to stacking faults also changes the shape of the reflections to more Lorentzian. The additional reflection observed at $2\theta = 7.49°$ may be the 100 reflection in the $R\bar{3}c$ cell, and this reflection is strongly asymmetric.

3.6. Structural Comparison between r-/c-$Ce(BH_4)_3$ and Other Metal Borohydrides. Analogous to cerium borohydride, samarium borohydride also crystallizes in different polymorphs, i.e., α-$Sm(BH_4)_3$, and β-$Sm(BH_4)_3$. In a recent study, both α-$Sm(BH_4)_3$ and β-$Sm(BH_4)_3$ were found at room temperature after ball milling.[37] The β polymorph of rare earth metal borohydrides usually crystallizes at higher temperatures.[36,37,40] A higher *V/Z* value is found for β-$Sm(BH_4)_3$ compared to α-$Sm(BH_4)_3$; see Table 1.[37] This is not the case for r-$Ce(BH_4)_3$ and c-$Ce(BH_4)_3$ and the *in situ* SR-PXD data reveal crystallization of r-$Ce(BH_4)_3$ at higher temperatures compared to c-$Ce(BH_4)_3$. Indeed, this illustrates that r-$Ce(BH_4)_3$ and c-$Ce(BH_4)_3$ cannot be described as low temperature/high temperature structural polymorphs.

The highly porous γ-$Mg(BH_4)_2$ is the first metal borohydride found to absorb guest molecules and has pore diameters above 7 Å; see Table 2.[49] The recently discovered γ-$Mn(BH_4)_2$ also contains large voids within the crystal structure.[41,50] Moreover, in the case of $Y(BH_4)_3$ the unit cell volume increases by 7% on the transition from α-$Y(BH_4)_3$ to β-$Y(BH_4)_3$. Thus, the high temperature β-$Y(BH_4)_3$ structure becomes noticeably more open, and it has large unoccupied voids at the position 1/4, 1/4, 1/4 with a distance from the center to the nearest hydrogen atom of 3.32 Å.[36,40] However, owing to the larger size of cerium compared to yttrium, the voids are considerably larger for c-$Ce(BH_4)_3$; see Table 2. On conversion of c-$Ce(BH_4)_3$ into r-$Ce(BH_4)_3$, the unit cell volume decreases significantly by 21%, and actually, r-$Ce(BH_4)_3$ is much denser compared to c-$Ce(BH_4)_3$; see the *V/Z* values in Table 1. An even larger volume reduction of 44% is observed for the transition from γ-$Mg(BH_4)_2$ to δ-$Mg(BH_4)_2$ at pressures above 1.1 GPa.[49] In c-$Ce(BH_4)_3$, the center of the void at 1/4, 1/4, 1/4 is 3.53 Å from the nearest hydrogen atom corresponding to void volume of 59 Å^3 (the latter is calculated in Platon software using van der Waals radii). This may be large enough to accommodate small molecules like H_2. The porosity is about 30%, which is similar to that of γ-$Mg(BH_4)_2$. However, the voids in c-$Ce(BH_4)_3$ are slightly smaller compared to γ-$Mg(BH_4)_2$.[49] Additionally, the volume change between c-$Ce(BH_4)_3$ and r-$Ce(BH_4)_3$ may be compared to the metal−organic framework, MIL-53, which also undergoes a structural transition from an open pore to closed pore structure as a function of guest entrance or temperature change.[51,52] Yet, since c-$Ce(BH_4)_3$ only appears in a limited temperature range, it may be a metastable intermediate, which only forms on removing the dimethyl sulfide molecules from the solvate, followed by a rapid collapse into the rhombohedral polymorph. Consequently, the gas absorption in c-$Ce(BH_4)_3$ can only be tested once the conditions to stabilize the open cubic phase at room temperature are found.

3.7. Reaction of r-$La(BH_4)_3$ with LiCl. After the extraction of $M(BH_4)_3$ (M = La, Ce) with $S(CH_3)_2$, the latter may be removed completely by a heating the samples in a vacuum. This allows us to study and use r-$M(BH_4)_3$ (M = La, Ce) without halide salts and $S(CH_3)_2$. Several recent works have reported halide salt and solvent free rare earth metal borohydrides, e.g., $Eu(BH_4)_2$,[29] $A(BH_4)_3$ (A = Y, Gd, Dy),[31,53,54] as well as perovskite and garnet structures containing rare earth metal borohydrides.[27,30,55] Here, we further show that r-$M(BH_4)_3$ (M = La, Ce) react with LiCl in the ratio 1:1 and thereby produces the solid-state lithium ion conductor $LiM(BH_4)_3Cl$ (M = La, Ce). This may seem counterintuitive, since the main objective of this work was to remove LiCl. However, the reaction between r-$M(BH_4)_3$ (M = La, Ce) and LiCl allows control over the amount of LiCl within the sample, i.e., the formation of phase pure samples, as well as opens the possibility to use other halide salts, e.g., AX or MgX_2 (A = Li, Na, K; X = F, Cl, Br, I), which may modify the conductivity of the resulting products. This opens the way to synthesize other members of the series potentially with Na- and Mg-ion conductivity. Additionally, r-$Ce(BH_4)_3$ have recently been used in the synthesis of the garnet-type trimetallic borohydride $Li_3K_3Ce_2(BH_4)_{12}$, which also shows high Li ion conductivity.[55] In the current example, the r-$La(BH_4)_3$-LiCl 1:1 mixture was ball milled, and the sample was heated during an *in situ* SR-PXD experiment from room temperature to 190 °C; see Figure 6. At room temperature, Bragg reflections from r-$La(BH_4)_3$ and LiCl are observed. At 97 °C, Bragg reflections from $LiLa(BH_4)_3Cl$ appear, while the intensity of Bragg reflections belonging to r-$La(BH_4)_3$ and LiCl begin to decrease. At 151 °C, r-$La(BH_4)_3$ is almost entirely consumed, and only a small amount of LiCl remains. At 175 °C, the Bragg reflections from $LiLa(BH_4)_3Cl$ also vanish. Therefore, $LiLa(BH_4)_3Cl$ may be synthesized by annealing a ball milled sample of $La(BH_4)_3$-LiCl 1:1 between 140 and 170 °C.

4. CONCLUSION

The synthesis of lanthanum and cerium borohydride has been performed in different solvents, and the products have been studied using thermal analysis and *in situ* SR-PXD. The reaction

DOI: 10.1021/acs.inorgchem.6b01526
Inorg. Chem. 2016, 55, 9748−9756

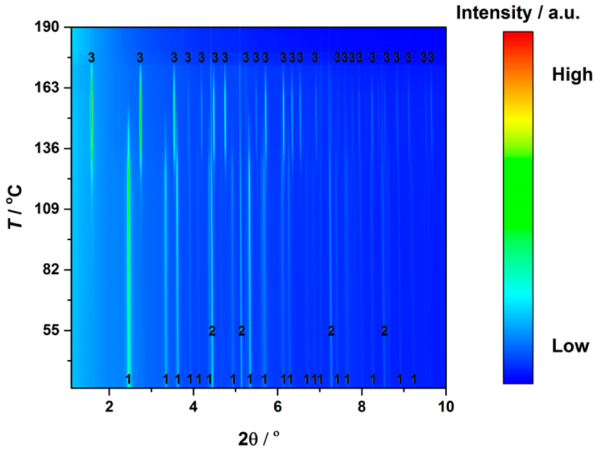

Figure 6. *In-situ* SR-PXD for $La(BH_4)_3$ + LiCl 1:1 (beamline P02.1, PETRA III, DESY, $\Delta T/\Delta t$ = 5 °C/min, p(Ar) = 1 bar, λ = 0.2309 Å). Symbols: **1**: r-$La(BH_4)_3$, **2**: LiCl, **3**: $LiLa(BH_4)_3Cl$.

between MCl_3 (M = La, Ce) and $LiBH_4$ in diethyl ether yields a solvate phase $LiM(BH_4)_3Cl{\cdot}Et_2O$ (M = La, Ce), which upon heating releases Et_2O and produces $LiM(BH_4)_3Cl$ (M = La, Ce) with a lower amount of LiCl as byproduct compared to the known mechanochemical synthesis. Alternatively, the reaction in toluene followed by extraction with dimethyl sulfide produces a solvate phase $M(BH_4)_3{\cdot}nS(CH_3)_2$ (M = La, Ce), which upon heating instead yields the monometallic ($R\bar{3}c$) borohydrides of lanthanum and cerium, r-$M(BH_4)_3$ (M = La, Ce). The two synthetic routes differ by the solubility of $LiBH_4$ in diethyl ether, which assists the incorporation of Li^+ and Cl^- in the reaction product. A cubic polymorph, c-$Ce(BH_4)_3$, with 21% larger unit cell volume as compared to r-$Ce(BH_4)_3$, was observed by *in situ* SR-PXD.

The rare earth metal borohydrides and the synthesis procedures described here may be used in the production of new solid-state ion conductors. The reaction pathway in diethyl ether can possibly be extended to other rare earth metal halides, e.g., reactions between MX_3 and $LiBH_4$ (M = La, Ce; X = Cl, Br, I). Furthermore, we performed the addition reaction between r-$La(BH_4)_3$ and LiCl resulting in the solid-state ion conductor $Li_4[La_4(BH_4)_{12}Cl_4]$. This reaction pathway may be extended to other metal halides such as NaCl, KCl, or $MgCl_2$ and/or bromides and iodides. This opens a way to synthesize other members of the series $A_4[M_4(BH_4)_{12}X_4]$ (A = Li, Na, K, Mg, M = La, Ce; X = Cl, Br, I) potentially showing Na- or Mg-ion conductivity.

■ ASSOCIATED CONTENT

Supporting Information

The Supporting Information is available free of charge on the ACS Publications website at DOI: 10.1021/acs.inorgchem.6b01526.

SR-PXD data from r-$La(BH_4)_3$ (Figure S1), SR-PXD data from $LiCe(BH_4)_3Cl{\cdot}nEt_2O$ (Figure S2), thermal analysis and mass spectrometry data $LiCe(BH_4)_3Cl{\cdot}nEt_2O$ (Figure S3), SR-PXD data from $La(BH_4)_3{\cdot}mS(CH_3)_2$ (Figure S4), thermal analysis data from $Ce(BH_4)_3{\cdot}nS(CH_3)_2$ (Figure S5), thermal analysis data from $Ce(BH_4)_3$ (Figure S6), thermal analysis data from $La(BH_4)_3{\cdot}nS(CH_3)_2$ (Figure S7), atomic positions for r-$Ce(BH_4)_3$ (Table S1), atomic positions for c-$Ce(BH_4)_3$ (Table S2) (PDF)

■ AUTHOR INFORMATION

Corresponding Authors

*(M.B.L.) E-mail: ley@mpi-muelheim.mpg.de. Tel: +49(0) 208/306-2369.
*(T.R.J.) E-mail: trj@chem.au.dk. Tel: +45 8942 3894. Fax: +45 8619 6199.

Notes

The authors declare no competing financial interest.

■ ACKNOWLEDGMENTS

We acknowledge the Danish Natural Science Research Councils for funding the research program DanScatt and The Innovation Fund Denmark (project HyFill-Fast). We also recognize Center for Materials Crystallography (CMC) funded by The Danish National Research Foundation for support. This work was supported by the Swiss National Science Foundation and Fonds de la Recherche Scientifique FNRS. We are grateful for the allocated beam time at ESRF, France, Diamond Light Source, UK, DESY, Germany, and The MAX IV laboratory, Sweden.

■ REFERENCES

(1) Howarth, R. W.; Ingraffea, A.; Engelder, T. Natural Gas: Should Fracking Stop? *Nature* **2011**, *477*, 271−275.
(2) Ley, M. B.; Jepsen, L. H.; Lee, Y.-S.; Cho, Y. W.; Bellosta von Colbe, J. M.; Dornheim, M.; Rokni, M.; Jensen, J. O.; Sloth, M.; Filinchuk, Y.; Jørgensen, J. E.; Besenbacher, F.; Jensen, T. R. Complex Hydrides for Hydrogen Storage − New Perspectives. *Mater. Today* **2014**, *17*, 122−128.
(3) Armand, M.; Tarascon, J.-M. Building Better Batteries. *Nature* **2008**, *451*, 652−657.
(4) Goodenough, J. B.; Kim, Y. Challenges for Rechargeable Li Batteries. *Chem. Mater.* **2010**, *22*, 587−603.
(5) Jepsen, L. H.; Ley, M. B.; Lee, Y.-S.; Cho, Y. W.; Dornheim, M.; Jensen, J. O.; Filinchuk, Y.; Jørgensen, J. E.; Besenbacher, F.; Jensen, T. R. Boron−nitrogen Based Hydrides and Reactive Composites for Hydrogen Storage. *Mater. Today* **2014**, *17*, 129−135.
(6) Ley, M.; Meggouh, M.; Moury, R.; Peinecke, K.; Felderhoff, M. Development of Hydrogen Storage Tank Systems Based on Complex Metal Hydrides. *Materials* **2015**, *8*, 5891−5921.
(7) Rude, L. H.; Nielsen, T. K.; Ravnsbæk, D. B.; Bösenberg, U.; Ley, M. B.; Richter, B.; Arnbjerg, L. M.; Dornheim, M.; Filinchuk, Y.; Besenbacher, F.; Jensen, T. R. Tailoring Properties of Borohydrides for Hydrogen Storage: A Review. *Phys. Status Solidi A* **2011**, *208*, 1754−1773.
(8) Bogdanović, B.; Schwickardi, M. Ti-Doped Alkali Metal Aluminium Hydrides as Potential Novel Reversible Hydrogen Storage Materials. *J. Alloys Compd.* **1997**, *253*−*254*, 1−9.
(9) Schlapbach, L.; Züttel, A. Hydrogen-Storage Materials for Mobile Applications. *Nature* **2001**, *414*, 353−358.
(10) Züttel, A.; Wenger, P.; Rentsch, S.; Sudan, P.; Mauron, P.; Emmenegger, C. $LiBH_4$ a New Hydrogen Storage Material. *J. Power Sources* **2003**, *118*, 1−7.
(11) Mazzucco, A.; Dornheim, M.; Sloth, M.; Jensen, T. R.; Jensen, J. O.; Rokni, M. Bed Geometries, Fueling Strategies and Optimization of Heat Exchanger Designs in Metal Hydride Storage Systems for Automotive Applications: A Review. *Int. J. Hydrogen Energy* **2014**, *39*, 17054−17074.
(12) Nakamori, Y.; Orimo, S. I.; Tsutaoka, T. Dehydriding Reaction of Metal Hydrides and Alkali Borohydrides Enhanced by Microwave Irradiation. *Appl. Phys. Lett.* **2006**, *88*, 112104.
(13) Matsuo, M.; Nakamori, Y.; Orimo, S. I.; Maekawa, H.; Takamura, H. Lithium Superionic Conduction in Lithium Borohydride Accompanied by Structural Transition. *Appl. Phys. Lett.* **2007**, *91*, 224103.

DOI: 10.1021/acs.inorgchem.6b01526
Inorg. Chem. 2016, 55, 9748−9756

(14) Matsuo, M.; Orimo, S. Lithium Fast-Ionic Conduction in Complex Hydrides: Review and Prospects. *Adv. Energy Mater.* **2011**, *1*, 161−172.
(15) Arnbjerg, L. M.; Ravnsbæk, D. B.; Filinchuk, Y.; Vang, R. T.; Cerenius, Y.; Besenbacher, F.; Jørgensen, J.-E.; Jakobsen, H. J.; Jensen, T. R. Structure and Dynamics for $LiBH_4$−LiCl Solid Solutions. *Chem. Mater.* **2009**, *21*, 5772−5782.
(16) Unemoto, A.; Chen, C.; Wang, Z.; Matsuo, M.; Ikeshoji, T.; Orimo, S. Pseudo-Binary Electrolyte, $LiBH_4$−LiCl, for Bulk-Type All-Solid-State Lithium-Sulfur Battery. *Nanotechnology* **2015**, *26*, 254001.
(17) Paskevicius, M.; Pitt, M. P.; Brown, D. H.; Sheppard, D. A.; Chumphongphan, S.; Buckley, C. E. First-Order Phase Transition in the $Li_2B_{12}H_{12}$ System. *Phys. Chem. Chem. Phys.* **2013**, *15*, 15825−15828.
(18) Udovic, T. J.; Matsuo, M.; Tang, W. S.; Wu, H.; Stavila, V.; Soloninin, A. V.; Skoryunov, R. V.; Babanova, O. A.; Skripov, A. V.; Rush, J. J.; Unemoto, A.; Takamura, H.; Orimo, S.-I. Exceptional Superionic Conductivity in Disordered Sodium Decahydro-Closo-Decaborate. *Adv. Mater.* **2014**, *26*, 7622−7626.
(19) Sadikin, Y.; Brighi, M.; Schouwink, P.; Černý, R. Superionic Conduction of Sodium and Lithium in Anion-Mixed Hydroborates $Na_3BH_4B_{12}H_{12}$ and $(Li_{0.7}Na_{0.3})_3BH_4B_{12}H_{12}$. *Adv. Energy Mater.* **2015**, *5*, 1501016.
(20) He, L.; Li, H.-W.; Nakajima, H.; Tumanov, N.; Filinchuk, Y.; Hwang, S.-J.; Sharma, M.; Hagemann, H.; Akiba, E. Synthesis of a Bimetallic Dodecaborate $LiNaB_{12}H_{12}$ with Outstanding Superionic Conductivity. *Chem. Mater.* **2015**, *27*, 5483−5486.
(21) Tang, W. S.; Unemoto, A.; Zhou, W.; Stavila, V.; Matsuo, M.; Wu, H.; Orimo, S.; Udovic, T. J. Unparalleled Lithium and Sodium Superionic Conduction in Solid Electrolytes with Large Monovalent Cage-like Anions. *Energy Environ. Sci.* **2015**, *8*, 3637−3645.
(22) Ley, M. B.; Ravnsbæk, D. B.; Filinchuk, Y.; Lee, Y.-S.; Janot, R.; Cho, Y. W.; Skibsted, J.; Jensen, T. R. $LiCe(BH_4)_3Cl$, a New Lithium-Ion Conductor and Hydrogen Storage Material with Isolated Tetranuclear Anionic Clusters. *Chem. Mater.* **2012**, *24*, 1654−1663.
(23) Ley, M. B.; Boulineau, S.; Janot, R.; Filinchuk, Y.; Jensen, T. R. New Li Ion Conductors and Solid State Hydrogen Storage Materials: $LiM(BH_4)_3Cl$, M = La, Gd. *J. Phys. Chem. C* **2012**, *116*, 21267−21276.
(24) Skripov, A. V.; Soloninin, A. V.; Ley, M. B.; Jensen, T. R.; Filinchuk, Y. Nuclear Magnetic Resonance Studies of BH_4 Reorientations and Li Diffusion in $LiLa(BH_4)_3Cl$. *J. Phys. Chem. C* **2013**, *117*, 14965−14972.
(25) Frommen, C.; Sørby, M. H.; Ravindran, P.; Vajeeston, P.; Fjellvåg, H.; Hauback, B. C. Synthesis, Crystal Structure, and Thermal Properties of the First Mixed-Metal and Anion-Substituted Rare Earth Borohydride $LiCe(BH_4)_3Cl$. *J. Phys. Chem. C* **2011**, *115*, 23591−23602.
(26) Černý, R.; Schouwink, P. The Crystal Chemistry of Inorganic Metal Borohydrides and Their Relation to Metal Oxides. *Acta Crystallogr., Sect. B: Struct. Sci., Cryst. Eng. Mater.* **2015**, *71*, 619−640.
(27) Schouwink, P.; Ley, M. B.; Tissot, A.; Hagemann, H.; Jensen, T. R.; Smrčok, L.; Černý, R. Structure and Properties of Complex Hydride Perovskite Materials. *Nat. Commun.* **2014**, *5*, 5706.
(28) Marks, S.; Heck, J. G.; Habicht, M. H.; Oña-Burgos, P.; Feldmann, C.; Roesky, P. W. $[Ln(BH_4)_2(THF)_2]$ (Ln = Eu, Yb)–a Highly Luminescent Material. Synthesis, Properties, Reactivity, and NMR Studies. *J. Am. Chem. Soc.* **2012**, *134*, 16983−16986.
(29) Humphries, T. D.; Ley, M. B.; Frommen, C.; Munroe, K. T.; Jensen, T. R.; Hauback, B. C. Crystal Structure and in Situ Decomposition of $Eu(BH_4)_2$ and $Sm(BH_4)_2$. *J. Mater. Chem. A* **2015**, *3*, 691−698.
(30) Schouwink, P.; Didelot, E.; Lee, Y. S.; Mazet, T.; Černý, R. Structural and Magnetocaloric Properties of Novel Gadolinium Borohydrides. *J. Alloys Compd.* **2016**, *664*, 378−384.
(31) Ley, M. B.; Paskevicius, M.; Schouwink, P.; Richter, B.; Sheppard, D. A.; Buckley, C. E.; Jensen, T. R. Novel Solvates $M(BH_4)_3S(CH_3)_2$ and Properties of Halide-Free $M(BH_4)_3$ (M = Y or Gd). *Dalton Trans.* **2014**, *43*, 13333−13342.
(32) Jaroń, T.; Orłowski, P. A.; Wegner, W.; Fijałkowski, K. J.; Leszczyński, P. J.; Grochala, W. Hydrogen Storage Materials: Room-Temperature Wet-Chemistry Approach toward Mixed-Metal Borohydrides. *Angew. Chem., Int. Ed.* **2015**, *54*, 1236−1239.
(33) Jaroń, T.; Wegner, W.; Fijałkowski, K. J.; Leszczyński, P. J.; Grochala, W. Facile Formation of Thermodynamically Unstable Novel Borohydride Materials by a Wet Chemistry Route. *Chem. - Eur. J.* **2015**, *21*, 5689−5692.
(34) Roedern, E.; Lee, Y.-S.; Ley, M. B.; Park, K.; Cho, Y. W.; Skibsted, J.; Jensen, T. R. Solid State Synthesis, Structural Characterization and Ionic Conductivity of Bimetallic Alkali-Metal Yttrium Borohydrides $MY(BH_4)_4$ (M = Li and Na). *J. Mater. Chem. A* **2016**, *4*, 8793−8802.
(35) Hagemann, H.; Longhini, M.; Kaminski, J. W.; Wesolowski, T. a; Černý, R.; Penin, N.; Sørby, M. H.; Hauback, B. C.; Severa, G.; Jensen, C. M. $LiSc(BH_4)_4$: A Novel Salt of Li^+ and Discrete $Sc(BH_4)_4^-$ Complex Anions. *J. Phys. Chem. A* **2008**, *112*, 7551−7555.
(36) Ravnsbæk, D. B.; Filinchuk, Y.; Černý, R.; Ley, M. B.; Haase, D.; Jakobsen, H. J.; Skibsted, J.; Jensen, T. R. Thermal Polymorphism and Decomposition of $Y(BH_4)_3$. *Inorg. Chem.* **2010**, *49*, 3801−3809.
(37) Olsen, J. E.; Frommen, C.; Jensen, T. R.; Riktor, M. D.; Sørby, M. H.; Hauback, B. C. Structure and Thermal Properties of Composites with RE-Borohydrides (RE = La, Ce, Pr, Nd, Sm, Eu, Gd, Tb, Er, Yb or Lu) and $LiBH_4$. *RSC Adv.* **2014**, *4*, 1570−1582.
(38) Dyuzheva, T. I.; Bendeliani, N. A.; Kabalkina, S. S. Compressibility and Polymorphism of ReO_3 at Pressures up to 30 GPa. *Sov. Phys. Dokl.* **1988**, *33*, 1−2.
(39) Biswas, K.; Muthu, D. V. S.; Sood, a K.; Kruger, M. B.; Chen, B.; Rao, C. N. R. Pressure-Induced Phase Transitions in Nanocrystalline ReO_3. *J. Phys.: Condens. Matter* **2007**, *19*, 436214.
(40) Frommen, C.; Aliouane, N.; Deledda, S.; Fonneløp, J. E.; Grove, H.; Lieutenant, K.; Llamas-Jansa, I.; Sartori, S.; Sørby, M. H.; Hauback, B. C. Crystal Structure, Polymorphism, and Thermal Properties of Yttrium Borohydride $Y(BH_4)_3$. *J. Alloys Compd.* **2010**, *496*, 710−716.
(41) Richter, B.; Ravnsbæk, D. B.; Tumanov, N.; Filinchuk, Y.; Jensen, T. R. Manganese Borohydride; Synthesis and Characterization. *Dalton Trans.* **2015**, *44*, 3988−3996.
(42) Jensen, T. R.; Nielsen, T. K.; Filinchuk, Y.; Jørgensen, J.-E.; Cerenius, Y.; Gray, E. M.; Webb, C. J. Versatile in Situ Powder X-Ray Diffraction Cells for Solid-Gas Investigations. *J. Appl. Crystallogr.* **2010**, *43*, 1456−1463.
(43) Hansen, B. R. S.; Møller, K. T.; Paskevicius, M.; Dippel, A.-C.; Walter, P.; Webb, C. J.; Pistidda, C.; Bergemann, N.; Dornheim, M.; Klassen, T.; Jørgensen, J.-E.; Jensen, T. R. In Situ X-Ray Diffraction Environments for High-Pressure Reactions. *J. Appl. Crystallogr.* **2015**, *48*, 1234−1241.
(44) Boultif, A.; Louër, D. Powder Pattern Indexing with the Dichotomy Method. *J. Appl. Crystallogr.* **2004**, *37*, 724−731.
(45) Favre-Nicolin, V.; Černý, R. FOX, 'free Objects for Crystallography': A Modular Approach to Ab Initio Structure Determination from Powder Diffraction. *J. Appl. Crystallogr.* **2002**, *35*, 734−743.
(46) Rodríguez-Carvajal, J. Recent Advances in Magnetic Structure Determination by Neutron Powder Diffraction. *Phys. B* **1993**, *192*, 55−69.
(47) Spek, A. L. Structure Validation in Chemical Crystallography. *Acta Crystallogr., Sect. D: Biol. Crystallogr.* **2009**, *65*, 148−155.
(48) Warren, B. E. *X-Ray Diffraction*, Reprint Ed.; Dover Publications, Mineola, NY, 1990; pp 1−400.
(49) Filinchuk, Y.; Richter, B.; Jensen, T. R.; Dmitriev, V.; Chernyshov, D.; Hagemann, H. Porous and Dense Magnesium Borohydride Frameworks: Synthesis, Stability, and Reversible Absorption of Guest Species. *Angew. Chem., Int. Ed.* **2011**, *50*, 11162−11166.
(50) Tumanov, N. A.; Roedern, E.; Łodziana, Z.; Nielsen, D. B.; Jensen, T. R.; Talyzin, A. V.; Černý, R.; Chernyshov, D.; Dmitriev, V.; Palasyuk, T.; Filinchuk, Y. High-Pressure Study of $Mn(BH_4)_2$ Reveals a Stable Polymorph with High Hydrogen Density. *Chem. Mater.* **2016**, *28*, 274−283.

DOI: 10.1021/acs.inorgchem.6b01526
Inorg. Chem. 2016, 55, 9748−9756

(51) Serre, C.; Millange, F.; Thouvenot, C.; Noguès, M.; Marsolier, G.; Louër, D.; Férey, G. Very Large Breathing Effect in the First Nanoporous chromium(III)-Based Solids: MIL-53 or CrIII(OH)·{O_2C-C_6H_4- CO_2}·{HO_2C-C_6H_4 -CO_2H}x·H_2Oy. *J. Am. Chem. Soc.* **2002**, *124*, 13519−13526.

(52) Liu, Y.; Her, J. H.; Dailly, A.; Ramirez-Cuesta, A. J.; Neumann, D. A.; Brown, C. M. Reversible Structural Transition in MIL-53 with Large Temperature Hysteresis. *J. Am. Chem. Soc.* **2008**, *130*, 11813−11818.

(53) Sadikin, Y.; Stare, K.; Schouwink, P.; Brix Ley, M.; Jensen, T. R.; Meden, A.; Černý, R. Alkali Metal - Yttrium Borohydrides: The Link between Coordination of Small and Large Rare-Earth. *J. Solid State Chem.* **2015**, *225*, 231−239.

(54) Jepsen, L. H.; Ley, M. B.; Černý, R.; Lee, Y.-S.; Cho, Y. W.; Ravnsbæk, D.; Besenbacher, F.; Skibsted, J.; Jensen, T. R. Trends in Syntheses, Structures, and Properties for Three Series of Ammine Rare-Earth Metal Borohydrides, $M(BH_4)_3 \cdot nNH_3$ (M = Y, Gd, and Dy). *Inorg. Chem.* **2015**, *54*, 7402−7414.

(55) Brighi, M.; Schouwink, P.; Sadikin, Y.; Černý, R. Fast Ion Conduction in Garnet-Type Metal Borohydrides $Li_3K_3Ce_2(BH_4)_{12}$ and $Li_3K_3La_2(BH_4)_{12}$. *J. Alloys Compd.* **2016**, *662*, 388−395.

DOI: 10.1021/acs.inorgchem.6b01526
Inorg. Chem. 2016, 55, 9748−9756